IRAQI JOURNAL OF APPLIED PHYSICS
Vol. 22, No. 1, January-March 2026, pp. 131-136

Evaluation of Environmentally Friendly Zinc Oxide Nanoparticles Synthesized Using *Carica papaya* Leaf Extract for Renewable Energy Applications

Sunday W. Balogun [1]
Hakeem O. Oyeshola [2]*
Sefiu A. Bello [1]
Hope K. Adewumi [2]
Yekinni K. Sanusi [2]

[1] Department of Materials Science and Engineering, Kwara State University Malete, Kwara State, Nigeria
[2] Department of Pure and Applied Physics, Ladoke Akintola University of Technology, Ogbomoso, Oyo State Nigeria
*Corresponding author: hooyeshola@lautech.edu.ng

This research explores the green synthesis of zinc oxide nanoparticles using *Carica papaya* leaf extract as a reducing agent. With a focus on developing reliable, eco-friendly, and cost-effective nanomaterial for device technologies, this sustainable method offers an alternative to conventional bulk material synthesis. Synthesized powder samples were characterized using XRD, FTIR, UV-Vis spectroscopy, SEM, EDX, and TEM. Spin-coating technique was used for thin-film deposition, while current-voltage properties were measured using a four-point probe system connected to a Keithley 2400 measurement unit and a solar simulator. Absorption peaks ranged from 299-382 nm as recorded from UV-visible, which is inferior to bulk material at 410 nm. The band gap energy was estimated to be 3.47 eV, resistance 5192.63 Ω, resistivity 132.0038 Ωm^{-1}, and conductivity 7.6×10^{-3} Sm^{-1} were determined. These results highlight ZnO nanoparticles potential for renewable energy and semiconductor applications.

Keywords: Green synthesis; Nanomaterials; Thin-film deposition; Renewable energy application
Received: 19 March 2025; Revised: 10 August; Accepted: 17 August; Published: 1 January 2026

1. Introduction

Zinc oxide (ZnO) compounds and zinc oxide-based materials have received greater attention in renewable energy technology [1,2]. ZnO is an n-type semiconductor that exhibits n-type conductivity which is an inorganic substantial [3] with high electron mobility finds application as a material for optoelectronic and electronic device technologies [4-6]. ZnO has been extensively researched as a material for many decades, owing to its high stability and low toxicity [7]. ZnO has a direct band gap in the near UV spectrum at room temperature (~3.3 eV). The extensive research on ZnO as a material has been attributed to its high abundance and unique properties such as chemical compatibility, durability, conductivity, and a broad range of radiation absorption, among others [8]. Metal oxide nanoparticle synthesis by plant extract route has gained importance over other methods of synthesis, such as chemical and physical methods, due to its simple economic processing, environmental friendliness, nontoxicity, and ease of fabrication, among others. The twenty-first century development of nanoscience and nanotechnology has led to the design and production of nanoscaled metal oxides that possess shape and size, allowing them to be used in electronics, energy conversion, laser diodes, photovoltaic, ultraviolet photodetectors, and renewable energy systems [9-13]. The plant extract synthesis method enhances metal ion conversion to metal oxides by extract acting both as capping or oxidizing and reducing agents [14-16].

In this work, *Carica papaya* leaf extract is used to synthesize ZnO to reduce metal ions to metal oxides by acting as a reducing agent. ZnO is biocompatible with the extract because it can bind to the surface of bulk ZnO. Production of metal oxide nanoparticles by green synthesis technique at industrial quantities remains a challenge yet to be fully exploited. The mechanisms of the formation of nanoparticles (NPs) during synthesis needed to be understood [17,18]. Publications on metal oxide green synthesis to produce nanoparticles are reported. Kanika et al. [19] reported the antifungal activity and antioxidant assay assessment properties of synthesized ZnO nanoparticles from *Carica papaya* leaf extract. Balogun et al. [20] reported the synthesis of ZnO nanoparticles using *Carica papaya* fresh leaf extract for anode buffer layers in solar cells. The thin films they fabricated exhibit high optical transparency with a band gap between 3.2 and 3.4 eV. Alam et al. [21] reported the Phyto synthesis of

manganese-doped ZnO nanoparticles using *Carica papaya* leaf extract. They obtained a nanoparticle crystallite size of 19.23 nm using x-ray diffraction, a hydrodynamic diameter of 135.1 nm, and a zeta potential of -33.36 eV. Also, the photocatalytic activity, antioxidant activity, and antimicrobial action of the Mn-Zn nanoparticles were assessed. Rathnasamy et al. [22] reported production of ZnO nanoparticles via leaf extracts of *Carica papaya*. They reported hexagonal wurtzite structure of nanoparticles with a particle diameter size of ~50 nm, and it gave an efficiency of 1.6% and a current density of 8.1 mA/cm^2 when used as a photoanode in dye-sensitive solar cells. Bhuiyan et al. [23] reported iron oxide nanoparticles produced with extract of *Carica papaya* leaf for photocatalysis and antibacterial property assessments. The reported result showed efficient photocatalytic degradation ability and exhibited moderate antibacterial efficiency. Nizamuddin et al. [24] used *Carica papaya* leaves to synthesize ZnO nanoparticles. Aqueous extract acted as a reducing agent as well as a stabilizing agent. Published articles on the electrical and photovoltaic property assessment of ZnO nanoparticles for renewable energy applications are scarce in the literature, which calls for more experimental and analytical research. The synthesized ZnO nanoparticles were analyzed by UV-visible spectroscopy, X-ray diffraction (XRD), Fourier-transform infrared spectroscopy (FTIR), and scanning electron microscopy (SEM). The optical, structural, morphological, chemical bond, functional group, and electrical results of the ZnO nanoparticles characterized are presented.

2 Experimental Procedures

The glass slides for the experimental procedure were locally purchased and thoroughly washed with liquid soap in an ultrasonic water bath, cleaned in ethanol, rinsed in deionized H_2O, dried inside an oven at 150°C, and subsequently cooled to 27°C. Zinc nitrate hexahydrate was used as a precursor supplied by Sigma Aldrich. Other chemicals and reagents were locally purchased. *Carica papaya* leaves, a popular cuisine in Nigeria, were harvested from the nearby farm.

Leaves of the *Carica papaya* plant were collected and dried at ambient room temperature for 10 days. 15 g of dried crushed powder was immersed in 500 mL of distilled water in a container placed on a magnetic stirrer for the duration of 1 h at 70°C to extract the bioactive compounds. The mixture was left to cool to expunge and remove residual unwanted materials and was then filtered to get a clear extracted solution free from impurities. The filtrates were then kept for use without further purification.

15.0 g of zinc nitrate hexahydrate precursor was homogenously stirred in a beaker containing 45 ml of *Carica papaya* extract using a magnetic stirrer for 5 hours. The obtained precipitates were filtered and washed with deionized water to remove residue. The sample obtained was dried at 70°C in an oven, but it was still an amorphous product; hence, temperature annealing at 500°C for 1 hour in a furnace was done and left to cool in the furnace [25-27]. The refined samples were crushed into powder for the UV-visible spectroscopy analysis for the synthesized ZnO nanoparticles. The deposition of synthesized ZnO nanoparticles was carried out using spin-coating technique and these nanoparticles were dissolved in ethanol and the spin-coater was set at a speed of 3000 rpm for 30 s which was deposited on the cleaned substrate surface. The thin-films fabricated on a glass substrate were annealed for 30 minutes at 100°C in an oven to evaporate organic chemicals and then characterized.

The crystal structural patterns were revealed by Rigaku XRD instrument. Functional groups were obtained with a BUK M530 FTIR spectrophotometer. Optical absorption was studied with an ASUV-6300PC UV-Visible spectrophotometer. A JOEL-JSM 7600F SEM was used to reveal the ZnO nanoparticles micrograph. Energy-dispersive x-ray spectroscopy (EDX) was utilized to reveal the purity and elemental composition of the prepared ZnO nanoparticles. Current-voltage characteristics measurement was done using a Four-Point Probe (FPP) system equipped with a Keithley 2400 source measurement unit.

3. Results and Discussion

Figure (1) depicts the UV-Vis absorption spectra of ZnO nanoparticles. The spectrum shows the absorption peaks from 299 to 390 nm. A careful observation shows the absorption peaks were maximums at the wavelength of 299 and 382 nm but are lower in comparison to the absorption with bulk size that occurred at 410 nm.

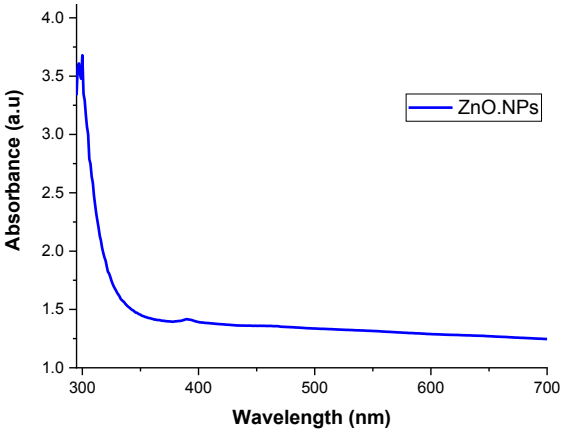

Fig. (1) UV-visible absorption spectrum of ZnO NPs

Figure (2) depicts the energy band gap analysis of the synthesized ZnO nanoparticles throughout the graphical relation plotted using the Tauc plot method

[28,29] by extrapolation of the linear portion of the graph $(\alpha hv)^2$ versus photon energy (hv) on the x-axis. Optical absorption coefficient (α) and photon energy (hv) are related by Eq. (1) for the direct transition of electrons from the valence band, which is filled with electrons to the conduction band which is empty as

$$(\alpha hv)^2 = A(hv - E_g) \quad (1)$$

where A stands for a constant, and E_g is the energy band gap in eV

The value of the energy band gap is 3.47 eV which concur with published study by Preethi et al. [30]. The energy band gap of ZnO nanoparticles depends on the bioactive compounds obtained from *Carica papaya* extract. The determined energy band gap is greater than that for bulk ZnO (3.3-3.7 eV) at ambient temperature [31,32]. This increase is attributed to the quantum confinement effect.

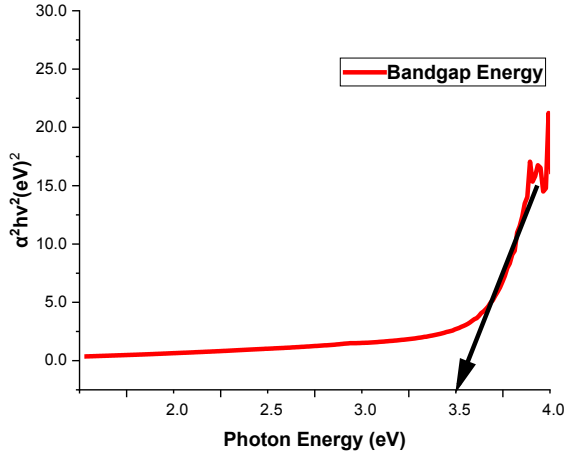

Fig. (2) determination of energy band gap of ZnO NPs

Figure (3) shows the XRD pattern of green synthesized ZnO nanopowder annealed at 500°C for 1 hour. This pattern indicates that the ZnO nanoparticles have a wurtzite hexagonal structure with peaks observed at 2θ of 38°, 41°, 43°, 51°, 57°, 62°, 66°, and 68° corresponding to Miller indices of (100), (002), (101), (102), (110), (103), (112), and (201), respectively. The sharp peaks observed indicate the high purity and crystallinity of ZnO nanoparticles. Annealing at 500°C influenced wurtzite hexagonal structure-oriented ZnO crystallites. The dominant peak at Miller indices of (101) corresponding to 2θ of 43° has the highest intensity, which indicates anisotropic growth and also indicates a preferred orientation of the crystallites. The crystallite size (D) was calculated by Debye-Scherrer's equation as:

$$D = \frac{K\lambda}{\beta \cos\theta} \quad (2)$$

where λ is the wavelength of X-ray radiation, K is a constant (shape factor), β is the full-width at half maximum (FWHM), and θ is the diffraction angle

The estimated crystallite size calculated using Eq. (2) is 35 nm. The diffraction pattern matched JCPDS card no. 89-7102. The result obtained is in agreement with published results reported by [19, 33].

Figure (4) indicates the FTIR spectrum of the synthesized ZnO nanoparticles. FTIR analysis was performed to investigate, determine, and identify the chemical bonds, vibrational stretching, and absorption bands of the synthesized nanoparticles. The single-bond vibrations between 2500 and 4000 cm^{-1} are ascribed to O-H, N-H, and C-H, the triple-bond vibrations are observed between 2000 and 2500 cm^{-1}, the double-bond vibrations from 1500 to 2000 cm^{-1} are attributed to C=C, C=O, and C=N, and the single-bond fingerprint vibration lies between 600 and 1500 cm^{-1} [34,35]. The peak observed at 3396.59 cm^{-1} involve both asymmetric and symmetric stretching modes of the hydroxyl group, H-bonded, and OH stretch (Zn-OH). The peaks at 3396.59 and 2628.20 cm^{-1} are characteristic of O-H bending modes of adsorbed water. The band centered at 2524.36 cm^{-1} is assigned to Thiols S-H stretch [34]. The band seen 1819.66 cm^{-1} belongs to the aromatic ring (aryl) functional group. The observed band peak at 1433.25 cm^{-1} belongs to Methyl C-H asymmetric/symmetric bend. The Zn-O stretching and Zn-O-Zn bridging stretching modes at 880.56 and 728.86 cm^{-1} in the fingerprint region confirm the formation of ZnO nanoparticles formation [36].

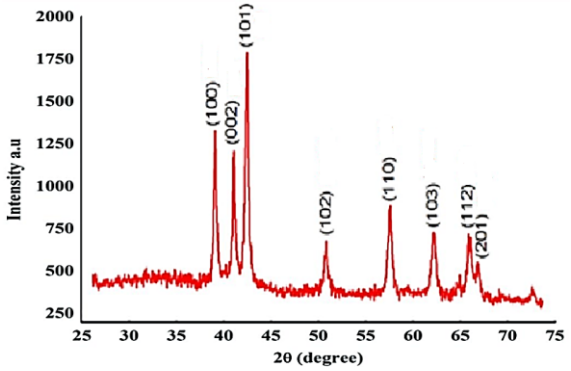

Fig. (3) XRD pattern of ZnO NPs synthesized in this work and annealed at 500°C

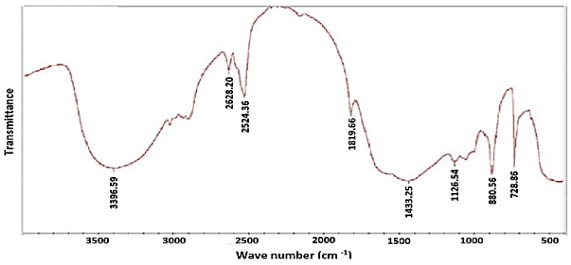

Fig. (4) FTIR spectrum of the synthesized ZnO NPs

Figure (5) shows SEM micrographs of ZnO nanopowders. The particle sizes in figures (5b,c, and d) are larger compared to Fig. (5a), which implies that annealing temperature at 500°C has improved the ability of ZnO nanoparticles to absorb photons from

solar spectrum, and hence decrease the resistivity and increase the conductivity of the material as the heat treatment produces electronic contacts between the nanoparticles. The EDX spectrum in Fig. (6) indicates the elemental composition of the synthesized ZnO nanoparticles. The elemental weight (%) composition of Zn (70.2%) and oxygen (13.0%) also successfully confirm the formation of ZnO nanoparticles. Other elements presented in the composition are assigned to the bioactive compounds of *Carica papaya* extract introduced during the synthesis process. Oxygen (O) must have been captured during synthesis process. Figure (7) shows the transmission electron microscopy (TEM) image at a scale of 100 nm. The particles are distinct and separate from each other and the size ranges from 35 to 87 nm showing a spherical geometry.

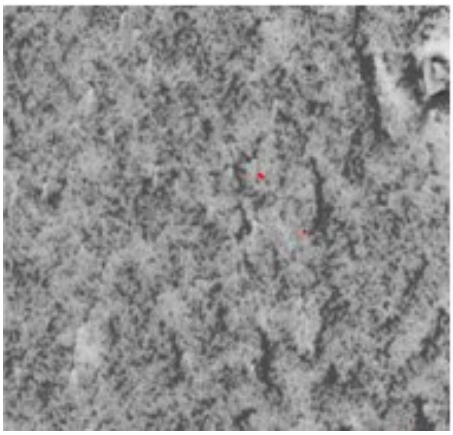

(a)

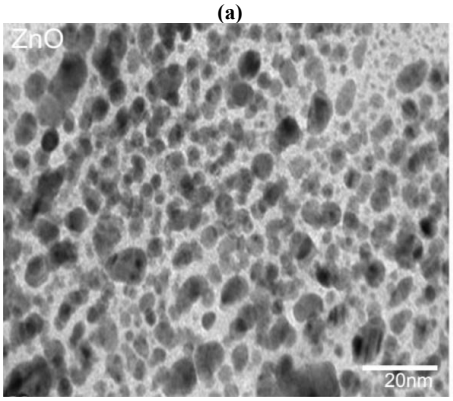

(b)

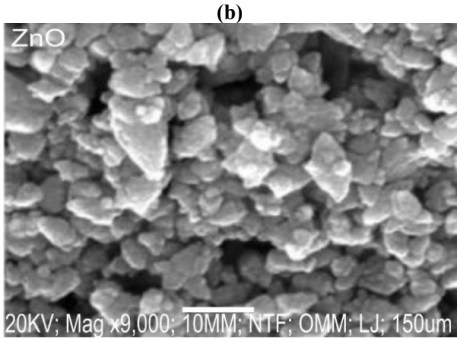

(c)

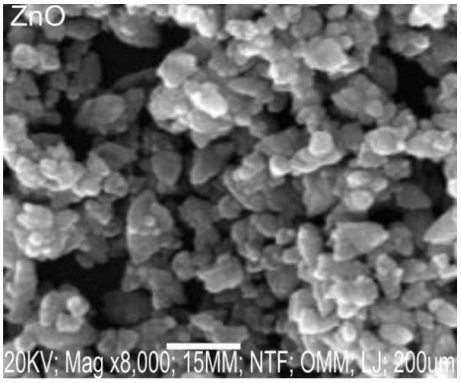

(d)

Fig. (5) SEM images of pure ZnO NPs (a) and ZnO NPs annealed at 500ºC (b) 20 nm, (c) 150 µm, (d) 200 µm magnifications

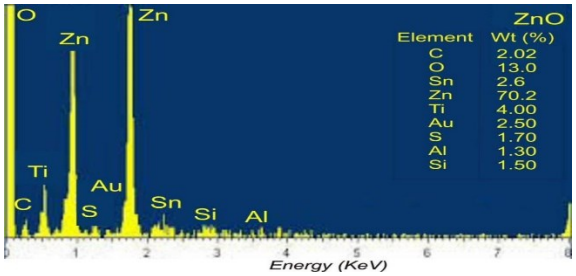

Fig. (6) EDX spectrum of the synthesized ZnO NPs

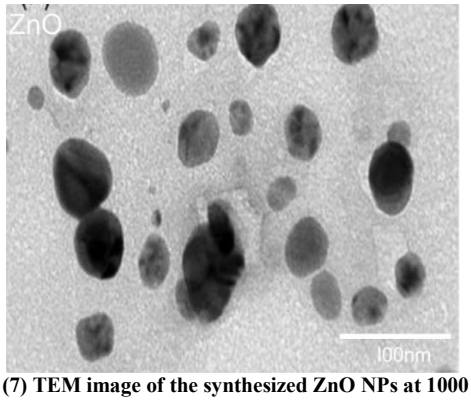

Fig. (7) TEM image of the synthesized ZnO NPs at 1000 nm

The current-voltage characteristics of ZnO nanoparticles deposited on an indium-doped tin oxide (ITO) substrate were measured using an FPP system equipped with a Keithley 2400 source meter and solar simulator. Figure (8) shows the schematic structure of the nanostructured ZnO thin film on ITO substrate and silver paste as a metal contact for I-V characteristics measurement. Figure (9) shows the obtained current-voltage characteristics. The resistance (R) was determined using the following equation

$$R = \frac{V}{I} \quad (3)$$

The resistance is related to the resistivity (ρ), cross-section area (a), and length (L) of the used substrate as follows:

$$R = \frac{\rho L}{a} \quad (4)$$

Resistivity (ρ) and conductivity (σ) are related by the following equation:

$$\sigma = \frac{1}{\rho} \quad (5)$$

The value of the resistance is 5192.63 Ω - which is relatively high - the resistivity of the nanoparticles was found to be 132.0038 Ω.m, and the conductivity was estimated to be 7.6x10^{-3} S/m.

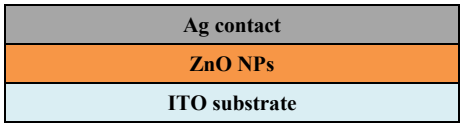

Fig. (8) Schematic diagram of the fabricated ZnO NPs-based device

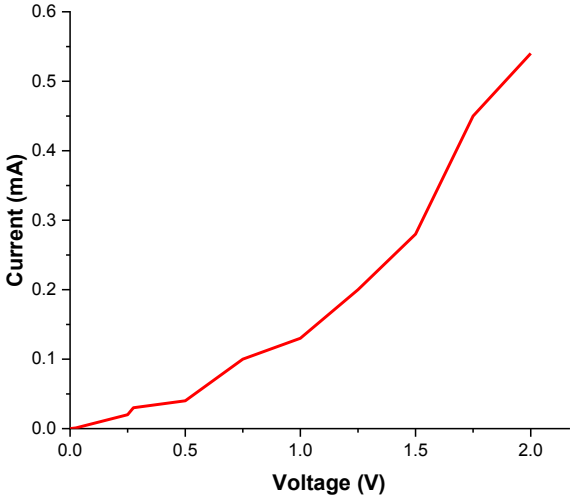

Fig. (9) Plot of current-voltage characteristics for ZnO NPs thin film device

4. Conclusions

In concluding remarks, the optical, structural, morphological and electrical properties of synthesized ZnO nanoparticles were presented. The maximum absorption peaks were noticeable within 299-390 nm with band gap of 3.47 eV. The synthesized nanoparticles showed wurtzite hexagonal structure with the highest intensity at miller indices (101). An electrical resistance of 5192.63 Ω, a resistivity of 132.0038 Ω.m, and a conductivity of 7.6x10^{-3} S/m were revealed. These combined promise properties show that the ZnO nanomaterial could perform better in renewable energy application.

Acknowledgments

The research was carried out at Materials Science & Engineering Department Laboratory, Kwara State University Malete, Nigeria. The authors therefore express their gratitude to Materials Science & Engineering Department for their moral support.

References

[1] W.J.D Xue, "Progress of science and technology of ZnO as advanced material", *Sci. Adv. Mater.*, 3(2) (2011) 127–149.

[2] S. Vyas, "A short review on properties and applications of zinc oxide based thin films and devices: ZnO as a promising material for applications in electronics, optoelectronics, biomedical and sensors", *Johnson Matthey Tech. Rev.*, 64(2) (2020) 202-218.

[3] S.W. Balogun et al., "Green synthesis and characterization of zinc oxide nanoparticles using bashful (Mimosa pudica), leaf extract: A precursor for organic electronics applications", *SN Appl. Sci.*, 2 (2020) 1-8.

[4] T. Yao, **"Zinc Oxide Encyclopedia of Materials: Science and Technology"**, Elsevier (Netherlands, 2001).

[5] S.C. Singh, "Zinc oxide nanostructures: Synthesis, characterizations and device applications", *J. Nanoeng. Nanomanufact.*, 3(4) (2013) 283–310.

[6] N. Koch, "Electronic structure of interfaces with conjugated organic materials", *phys. Stat. sol. (RRL): Rapid Res. Lett.*, 6(7) (2012) 277-293.

[7] M. Hadis and Ö. Ümit, **"ZnO Oxide Fundamentals, Materials and Device Technology"**, Willey-VCH Verlag GmbH (Weinheim, 2009).

[8] A. Sirelkhatim et al., "Review on zinc oxide nanoparticles: Antibacterial activity and toxicity mechanism", *Nano Micro Lett.*, 7(3) (2015) 219–242.

[9] N. Matinise et al., "Green synthesis of novel zinc iron oxide ($ZnFe_2O_4$) nanocomposite via *Moringa Oleifera* natural extract for electrochemical applications", *Appl. Surf. Sci.*, 446 (2018) 66–73.

[10] V. Helan et al., "Neem leaves mediated preparation of NiO nanoparticles and its magnetization, coercivity and antibacterial analysis", *Results Phys.*, 6 (2016) 712–718.

[11] S. Khamlich et al., "High performance symmetric supercapacitor based on zinc hydroxychloride nanosheets and 3D graphene-nickel foam composite", *Appl. Surf. Sci.*, 405 (2017) 329–336.

[12] G. Anandha Babu et al., "Influence of microwave power on the preparation of NiO nanoflakes for enhanced magnetic and supercapacitor applications", *Dalt. Trans.*, 44 (2015) 4485–4497.

[13] S. Iravani, "Green synthesis of metal nanoparticles using plants", *Green Chem.*, 13 (2011) 2638–2650.

[14] H.R. Vasanthi, N. ShriShriMal and D.K. Das, "Phytochemicals from Plants to Combat Cardiovascular Disease", *Curr. Med. Chem.*, 19 (2012) 2242–2251.

[15] G.G.F. Nascimento et al., "Antibacterial activity of plant extracts and phytochemicals on antibiotic-

resistant bacteria", *Brazilian J. Microbiol.*, 31 (2000) 247–256.
[16] S.W. Balogun et al., "Synthesis, characterization, and optoelectronic properties of zinc oxide nanoparticles: A precursor as electron transport layer", *Heliyon*, 10(9) (2024) e29452.
[17] M. Bandeira et al., "Green synthesis of zinc oxide nanoparticles: A review of the synthesis methodology and mechanism of formation", *Sustain. Chem. Pharm.*, 15 (2020) 100223.
[18] V.V. Makarov et al., "Green nanotechnologies: Synthesis of metal nanoparticles using plants", *Acta Naturae*, 6(1) (2014) 20–44.
[19] K. Dulta et al., "Ecofriendly Synthesis of Zinc Oxide Nanoparticles by *Carica papaya* Leaf Extract and Their Applications", *J. Cluster Sci.*, 33 (2021) 603-617.
[20] U.O. Aigbe and O.A. Osibote, "Green synthesis of metal oxide nanoparticles, and their various applications", *J. Hazard. Mater. Adv.*, 13 (2024) 100401.
[21] M.W. Alam et al., "Phytosynthesis of Manganese-Doped Zinc Nanoparticles Using *Carica papaya* Leaves: Structural Properties and Its Evaluation for Catalytic, Antibacterial and Antioxidant Activities", *Polymers,* 14 (2022) 1827.
[22] R. Rathnasamy et al., "Green synthesis of ZnO nanoparticles using *Carica papaya* leaf extracts for photocatalytic and photovoltaic applications", *J. Mater. Sci.: Mater. Electron.,* 28 (2027) 10374-10381.
[23] Md.S.H. Bhuiyan et al., "Green synthesis of iron oxide nanoparticle using *Carica papaya* leaf extract: application for photocatalytic degradation of remazol yellow RR dye and antibacterial activity", *Heliyon,* 6 (2020) e04603.
[24] S. Nizamuddin et al., "Green synthesis and characterization of ZnO nanoparticles-A novel approach using *Carica papaya* leaf extract", *Mater. Today Proc.*, 62 (2022) 6854-6856.
[25] M.K. Ahmad et al., "Effect of annealing temperatures on surface morphology and electrical properties of titanium dioxide thin films prepared by sol-gel method", *J. Sustai. Ener. Enviro.*, 1: (2010) 17-20.
[26] Z.W. Zhao and B.K. Tay, "Study of nanocrystal TiO_2 thin film by thermal annealing", *J. Electro. Ceram.*, 16 (2006) 489-493.
[27] D.J. Won et al., "Effects of thermally induced anatase-to-rutile phase transition in MOCVD-grown TiO_2 on structural and optical properties", *Appl. Phys. A,* 73 (2001) 595-600.
[28] J. Tauc, R. Grigorovici and A. Vancu, "Optical properties and electronic structure of amorphous germanium", *phys. stat. sol. (b)*, 15(2) (1966) 627–637.
[29] J. Tauc, **"The Optical Properties of Solids"**, North-Holland (Amsterdam, 1970).
[30] S. Preethi, A. Anitha and M. Arulmozhi, "A comparative analysis of the properties of zinc oxide (ZnO) nanoparticles synthesis by hydrothermal and sol-gel methods", *Indian J. Sci. Technol.*, 9(40) (2016) 1-6.
[31] B.D. Ngom et al., "ZnO nano-discs by lyophilization process: Size effects on their intrinsic luminescence", *J. Alloys Compd.*, 656 (2016) 758–763.
[32] K.M. Dooley, S.Y. Chen and J.R.H. Ross, "Stable Nickel-Containing Catalysts for the Oxidative Coupling of Methane", *J. Catal.*, 145 (1994) 402–408.
[33] J. Santhoshkumar, S.V. Kumar and S. Rajeshkumar, "Synthesis of zinc oxide nanoparticles using plant leaf extract against urinary tract inflection pathogen", *Resour. Efficient Technol.*, 3(4) (2017) 459-465.
[34] J. Coates, "Interpretation of infrared spectra, a practical approach", *Encyclo. Anal. Chem.*, 12 (2000) 10815-10837.
[35] A.B.D. Nandiyanto, R. Oktiani and R. Ragadhita. "How to Read and Interpret FTIR Spectroscope of Organic Material", *Indonesian J. Sci. Technol.,* 4(1) (2019) 97-118.
[36] S. Pai et al., "Synthesis and characterization of ZnO nanoparticles using moringa oleifera leaf extract: Investigation of photocatalytic and antibacterial activity", *Int. J. Nanosci. Natechnol.,* 14 (2018) 111-119.

